ACS Infectious Diseases

Article

Anti-tuberculosis activity of the anti-malaria cytochrome bcc oxidase inhibitor SCR0911

Sherilyn Chong, Malathy Sony Subramanian Manimekalai, Jickky Palmae Sarathy, Zoe C. Williams, Liam K. Harold, Gregory M Cook, Thomas Dick, Kevin Pethe, Roderick Wayland Bates, and Gerhard Grüber

ACS Infect. Dis., **Just Accepted Manuscript** • DOI: 10.1021/acsinfecdis.9b00408 • Publication Date (Web): 24 Feb 2020

Anti-tuberculosis activity of the anti-malaria cytochrome bcc oxidase inhibitor SCR0911

Chong Shi Min Sherilyn[1,2,3], Malathy Sony Subramanian Manimekalai[1], Jickky Palmae Sarathy[4], Zoe C. Williams[5], Liam K. Harold[5], Gregory M. Cook[5], Thomas Dick[4,6], Kevin Pethe[1,7], Roderick W. Bates[2,] and Gerhard Grüber[1,]*

[1]School of Biological Sciences, Nanyang Technological University, 60 Nanyang Drive, Singapore 637551, Republic of Singapore

[2]School of Physical and Mathematical Sciences, Nanyang Technological University, 21 Nanyang Link, Singapore 637371, Republic of Singapore

[3]Nanyang Institute of Technology in Health and Medicine, Interdisciplinary Graduate School, Nanyang Technological University, Republic of Singapore

[4]Department of Microbiology and Immunology, Yong Loo Lin School of Medicine, National University of Singapore, 14 Medical Drive, Singapore 117599, Republic of Singapore

[5]Department of Microbiology and Immunology, School of Biomedical Sciences, University of Otago, Dunedin 9054, New Zealand

[6]Center for Discovery and Innovation, Hackensack Meridian Health, 340 Kingsland Street Building 102, Nutley, NJ 07110, USA

[7]Lee Kong Chian School of Medicine, Nanyang Technological University, Singapore, 636921, Singapore

*To whom correspondence should be addressed: Prof. Dr. Gerhard Grüber, Tel.: (65) 6316 2989; E-mail: ggrueber@ntu.edu.sg

The ability to respire and generate ATP is essential for the physiology, persistence and pathogenicity of *Mycobacterium tuberculosis*, which causes Tuberculosis. By employing a lead repurposing strategy, the malarial cytochrome bc_1 inhibitor SCR0911 was tested against mycobacteria. Docking studies were carried out to reveal potential binding and to understand the binding interactions with the target, cytochrome *bcc*. Whole cell-based and *in vitro* assays demonstrated the potency of SCR0911 by inhibiting cell growth and ATP synthesis in both the fast- and slow- growing *M. smegmatis* and *M. bovis* bacillus Calmette–Guérin, respectively. The variety of biochemical assays and the use of a cytochrome *bcc*-deficient mutant strain validated the cytochrome *bcc* oxidase as the direct target of the drug. The data demonstrate the broad-spectrum activity of SCR0911 and opens the door for structure-activity relationship studies to improve the potency of new mycobacteria specific SCR0911 analogs.

Key Words: Tuberculosis, Mycobacteria, OXPHOS pathway, Multi Drug Resistance, Extremely Drug Resistance, Telacebec, Q203

Tuberculosis (TB) is one of the deadliest contagious diseases. [1] In 2018, there were 1.4 million deaths due to TB.[2] The current treatment of TB mainly utilizes a combination of antibiotics that requires long-term therapy. [3-5] This results in the emergence of multidrug-resistant TB (MDR-TB) and extensively drug-resistant TB (XDR-TB), which are difficult to manage and treat.[6-8]

There has been a recent resurgence of activity with a number of new compounds in the TB-drug pipeline, including promises of respiration by the electron transport chain (ETC) and ATP synthesis (oxidative phosphorylation) as new target spaces for drug development since the generation of ATP is essential for the bacterial pathogen's physiology, persistence and pathogenicity.[9] For example, clofazimine, which affects non-proton translocating NADH dehydrogenase (type II) of the ETC, is an antimycobacterial agent with good *in vitro* activity.[10] Telacebec (Q203), a cytochrome *bcc-aa*$_3$ terminal oxidase complex inhibitor is a bacteriostatic drug against *Mtb*.[11] The concept that oxidative phosphorylation inhibitors could shorten the time of therapy for drug-resistant tuberculosis is supported by the clinical development of Sirturo® (bedaquiline, BDQ), a drug targeting the *Mtb* F_1F_O ATP synthase. [12, 13] The cyt-*bcc-aa3* is required for optimum mycobacterial growth but is not strictly essential.[14] However, given the safety profile of the most advanced inhibitors demonstrated in human clinical trial phase 1 and 2, the synergy between Telacebec and inhibitors of the oxidative phosphorylation pathway,[15-17] and the synthetic lethal interaction between cyt-*bcc-aa3* and the cytochrome *bd* oxidase (cyt-*bd*),[15, 18] drugs targeting the cyt-*bcc-aa3* probably have their place in a rational drug combination for drug-resistant tuberculosis.

Mycobacteria harbour a number of primary dehydrogenases to fuel the ETC, and two terminal respiratory oxidases, an *aa*$_3$-type cytochrome *c* oxidase (cyt-*bcc-aa3*) and a bacterial-specific cytochrome *bd*-type menaquinol oxidase (cyt-*bd*). These are present for dioxygen reduction coupled to the generation of a proton motive force (PMF, the sum of

proton-gradient and the membrane potential), which is finally used for the condensation of ADP + P_i to form ATP by the engine F_1F_O-ATP synthase (F-ATP synthase).[19] Cyt-*bcc*, complex III of the ETC, aids in the transfer of electrons from menaquinol to cytochrome aa_3, known as the complex IV of the ETC, in which reduction of oxygen to water occurs. Cytochrome *bcc* consists of a Q_o and Q_i binding pocket, menaquinol is oxidized to menaquinone in the Q_o site, releasing protons which contribute to the generation of the PMF. Menaquinone binds to the Q_i site and becomes reduced in the process, to regenerate menaquinol.[20, 21] Besides cytochrome *bcc*, *Mtb* also possesses a cyt-*bd*, which is as a non-proton translocating terminal oxidase with functional importance under hypoxia *in vitro* and *in vivo*. [22-26]

There is growing evidence for the potential to repurpose drugs originally developed for the treatment of other diseases, for example clofazimine, for use against drug-resistant TB.[27, 28] Evidence for successful repurposing of antimalaria compounds for treating TB has been seen previously with triclosan, effective against wild-type and drug-resistant strains of *Mtb* and *Plasmodium falciparum*, the causative agent of malaria, by inhibiting the enoyl acyl carrier protein reductase [29]. Previously, it was uncovered that 4-(1H)- quinolone, such as SCR0911, are potent antimalarial compounds that target the cytochrome bc_1 of *P. falciparum*.[30, 31] The same authors have prepared a homology model of the *P. falciparum* cyt-bc_1, proposing SCR0911-binding and its derivatives to the Q_i site of the complex (Fig. 1). [30, 31] Recently, a crystal structure of the bovine cytochrome bc_1 confirmed binding of SCR0911 in the Q_i site, although differences were noted in the orientation and amino acids involved compared to the one within the *P. falciparum* complex (Fig. 1B), which may also reflect the lower potency of SCR0911 against the human enzyme.[30, 32]

SCR0911 has an encouraging anti-malarial activity of 12 nM, with a low inhibition to bovine heart bc_1, supporting the lower potency of SCR0911 against human enzyme.[30]

Although the *P. falciparum* and human cyt-bc_1 amino acids, which are proposed to be involved in SCR0911-binding, are not conserved in *Mycobacterium* species, except for residue G38 (Fig. 1B), with the low potency of SCR0911, along with the cryo-EM and crystal structure of SCR0911 with bovine cytochrome bc_1, we investigated herein whether SCR0911 could bind to the mycobacterial cyt-*bcc* complex, and whether such interactions would have sufficient potency to inhibit oxidative phosphorylation and bacterial growth.

RESULTS AND DISCUSSION

Docking of SCR0911 with *Mtb* cyt-*bcc* complex

In order to study the potential binding site and binding mode of SCR0911 in *Mtb* cyt-*bcc*, docking studies were carried out. Since the structure of *Mtb* cyt-*bcc* complex was not available, a homology model was generated based on the *M. smegmatis* Electron Microscopy (EM) structure (PDB ID: 6ADQ) as a template as described in Material and Methods.[21] The sequence identity between *Mtb* and *M. smegmatis* is high (81% for QcrA, 83% for QcrB and 80% for QcrC), therefore, a good model could be predicted with a sequence coverage of around 90%, 97% and 80%, and a GMQE (Global Model Quality Estimation) of around 0.76, 0.90 and 0.68 for QcrA, B and C, respectively. The *Mtb* model subunits are structurally very similar to the template *M. smegmatis* structures with r.m.s. deviation of 0.061, 0.063 and 0.069Å for QcrA, QcrB and QcrC, respectively. The individual subunits were assembled, and a dimer model was generated based on the *M. smegmatis* structure, which was then used to identify the binding region of SCR0911 (Supplementary Figure S1A and Fig. 2A-D). As the binding region of SCR0911 in *Mtb* cyt-*bcc* is unknown, the whole model was used for searching. 100 protein-ligand complex configurations were generated and analyzed. Clustering analysis revealed multiple binding sites of the compound in the *Mtb* cyt-*bcc* model with major and minor populations. Overlapping of the two monomers of the dimer revealed

two major and two minor binding sites with populations of 33% and 21% as well as 13% and 8%, respectively. Multiple site binding of the compound is expected, since the substrate menaquinone has three more binding sites in addition to the known two Q-sites in the *M. smegmatis* cyt-*bcc* structure.[21] The first major binding site with 33% population of the *Mtb cyt-bcc*-SCR0911 complex configuration lies on both QcrB and QcrC subunits through hydrophobic interactions, which were largely contributed from QcrB (Fig. 2A). This complex configuration has a free energy of binding of -7.01 kcal/mol with a theoretical inhibition constant (K_i) of 7.26 μM. In this complex configuration, SCR0911 is closer to high-spin heme (7.1 Å) and binds near the Q_o-site, the closest distance being 3.6 Å with F308 (Fig. 2A). The quinolone moiety of SCR0911 has a π-π interaction with W262 of QcrA and is stabilized by hydrophobic interactions with M259 of QcrA and Y389 and M390 of QcrB. F308 of QcrB stabilizes the methoxy group and M126 of QcrB stabilizes the pyridine ring. L349 and I386 of QcrB stabilizes the trifluoromethoxyphenyl group through hydrophobic interactions. Since SCR0911 binds in such a way that it covers the Q_o-site from behind, we assume that it affects the region near the Q_o-site. As it is closer to the heme, it might also indirectly influence the electron transfer pathway between the heme, thereby contributing to the inhibition of the enzyme (Fig. 2B). Moreover, the compound binds exactly at the menaquinone-binding site, although this position is reported to be a functionally irrelevant region. The large population of SCR0911 binding to this pocket might indicate that this binding region is significant, which needs to be evaluated in the future (Fig. 2B).[21] The second major binding site with a population of 21%, has interactions with all three subunits, viz. QcrA, B and C, with residues from subunits B and C contributing more to the interaction (Supplementary Figure 1B). Although largely hydrophobic interactions are observed, a hydrogen bond with S133 of QcrA is noted (Supplementary Figure 1C). The free energy of binding is -5.54 kcal/mol with a theoretical K_i of 86.78 μM. In this position, the compound is farther away from all the heme

molecules in the complex (distance from low and high spin heme in QcrB is 17.5 and 29.6 Å, respectively, and heme cD2 in QcrC is 17.2 Å away) and also from the Q_i and Q_o-site (21.0 Å and 25.6 Å, respectively). SCR0911 is not close to any of the menaquinone-binding sites, therefore, the importance of this position and the possible mechanism of action could not be deduced.

Of the two minor binding sites, the first one has a population of 13% and interacts through hydrophobic interactions with subunits QcrA and B and has a free energy of binding of -5.94 kcal/mol with the theoretical K_i of 44.40 μM (Supplementary Figure 1D, E). While the compound is not close to any of the heme molecules or to the Q-sites or the menaquinone sites, its proximity to the iron-sulfur (2Fe-2S) cluster in subunit QcrA (10.9 Å) might be relevant, as binding of SCR0911 at this position may affect the residues close to this cluster and thereby indirectly provide inhibition to the complex (Supplementary Figure 1F). The second minor binding site with a population of 8% is an important site as SCR0911 binds exactly in the Q_i-site (Fig. 2C). It has a free energy of binding of -5.75 kcal/mol with a theoretical K_i of 61.10 μM. The compound is closer to a high-spin heme (3.2 Å) and has hydrophobic interactions with residues of subunit QcrB (Fig. 2D). The oxygen atom of the quinolone moiety has a weak hydrogen bond interaction with Y53 and the methoxy group is stabilized by hydrophobic interaction with L52, H240 and F45. The pyridine ring has face-to-face π-interaction with W236 and the trifluoromethoxyphenyl group is stabilized by L31, L35 and Q34. Hence in this complex configuration, binding of SCR0911 in the Q_i-site and near the heme affects both menaquinone binding and influences the electron transfer pathway, thereby leading to inhibition of the complex (Fig. 2C & D). This complex configuration position is similar to the binding of the compound in the structure of bovine cyt-bc_1 complex (Fig. 2E).[32] However, the trifluoromethoxyphenyl pyridine moiety orients in a different direction although the quinolone moiety binds to a similar position. This differential binding

could be caused by the structural variations near the Q_i-site and the changes near the N-terminal helices of the *Mtb* and bovine qcrB subunit (Fig. 2E). The helix holding W236 of the Q_i-site, is moved inward, which pushes the 2nd helix from the N-terminus down in *Mtb* QcrB subunit. These structural variations create a wide space near the Q_i-site and allow a larger movement and the differential binding of the compound. The differential binding mode is not uncommon, as it has previously been reported that in the structure of bovine cyt-bc_1 complex the two potent antimalarial agents *in vivo*, SCR0911 and GSK932121, bind in the same Q_i-site but with a different binding mode.[31, 32]

Antimycobacterial activity of SCR0911

An alternative synthesis protocol for SCR0911 was established (Material and Methods and Fig. 3) to study the effect of the compound on mycobacterial growth and energetics. The modified scheme allows the direct synthesis of an oxazole directly from a carboxylic acid.[30] In the synthesis scheme by Charoensutthivarakul et al. (2015), an isatoic anhydride was first prepared from the carboxylic acid **6** using triphosgene, which will in turn be used to synthesize the oxazole **4** (Fig. 3). With the direct synthesis of the oxazole **4** directly from a carboxylic acid **6**, the synthesis was shortened and the use of triphosgene eliminated.

To gain a preliminary indication of the effectiveness of SCR0911 on mycobacteria, a growth inhibitory assay was carried out on both *M. bovis* BCG and *M. smegmatis* by assessing MIC values. As shown in Figure 4A, the MIC_{50} of BDQ for *M. smegmatis* was comparable with those reported (17 ± 2.3 nM), and an MIC_{50} of 188 ± 14 nM was found for *M. bovis* BCG (Fig. 4B).[15, 16, 33] The MIC_{50} of SCR0911 was determined to be 272 ± 41 μM and 107 ± 5.8 μM against *M. smegmatis* (Fig. 4A) and *M. bovis* BCG (Fig. 4B), respectively. As SCR0911 is proposed to bind to the cytochrome *bcc*, the *M. smegmatis* Δ*bcc* mutant strain ZCW111 was studied with BDQ as a negative control. The MIC_{50} of BDQ was 16 nM ± 1.9

(Fig. 4C) which is similar to the MIC_{50} of BDQ in WT *M. smegmatis* (17 nM ± 2.3). Like the mycobacterial *bcc*-inhibitor Telacebec. SCR0911 was unable to inhibit the growth of the Δ*bcc* mutant strains at the highest tested concentration (800 μM)(Fig. 4C), indicating that the compound may inhibit cell growth by interferring with the function of the cytochrome *bcc*. To further determine if SCR0911 targets the respiratory chain specifically, in-vitro assays were carried out.

SCR0911 triggers a rapid intracellular ATP depletion in mycobacteria.

To determine if the anti-mycobacterial activity is due to oxidative phosphorylation inhibition, an intracellular ATP synthesis assay was carried out on *M. bovis* BCG (Fig 4D). The IC_{50} of Telacebec and BDQ was found to be 0.5 ± 0.03 nM and 29 ± 2.7 nM, respectively, similar to the reported IC_{50} values in *Mtb* H37Rv.[11] Under similar conditions, SCR0911 had an effect on ATP levels at an IC_{50} of 50 ± 6.7 μM, indicating its ability to inhibit ATP synthesis.

To gain more insights into the inhibition of ATP synthesis, and to uncover the target of SCR0911, ATP synthesis was measured in inverted membrane vesicles (IMVs) in the presence of the electron donor NADH. The IC_{50} values obtained from the IMVs of *M. smegmatis* and *M. bovis* BCG were 7.6 ± 0.4 μM and 6.9 ± 1.4 μM, respectively (Fig. 5A-B). These IC_{50} values for both strains indicate its ability to bind to its target the cytochrome *bcc* complex in the oxidative phosphorylation pathway, which ultimately reduces ATP synthesis. Interestingly, the higher IC_{50} (IC_{50} = 50 ± 6.7 μM) observed for the intracelluar ATP synthesis inhibition by SCR0911 above might reflect a phenomenon observed for BDQ and Telacebec, whose inhibition of the F-ATP synthase and cyt*bcc*-aa_3 oxidase, respectively, causes an activation of the respiration of *M. tuberculosis* and *M. smegmatis* leading to dysregulation of mycobacterial metabolism.[5, 25, 34]

The results obtained from the IMVs motivated the use of purer IMVs, which were generated according to a recent protocol including two additional ultracentrifugation steps.[35] ATP synthesis initiated with NADH were carried out on these PMVs, and the IC_{50} obtained (3.8 ± 0.3 μM) was comparable to that of the IMVs (Fig. 5C). To determine if SCR0911 may affect the NADH-dehydrogenase or the succinate-dehydrogenase, a similar experiment was carried out using succinate instead of NADH, as succinate is taken up directly by complex II of the ETC. Telacebec was employed in this experiment as a positive control as it binds to the cytochrome *bcc* complex.[11] The IC_{50} obtained for Telacebec with NADH (1.1 ± 0.8 nM) and succinate (2.0 ± 0.1 nM) as the electron donor was comparable (Fig. 5C and D). Similarly for SCR0911, the IC_{50} was 3.4 ± 0.8 μM with succinate, alike to using NADH as a substrate (Fig. 5D). Hence, it can be inferred that SCR0911 does not inhibit the NADH-dehydrogenase nor the succinate dehydrogenase.

In parallel, a possible effect of SCR0911 on the respiratory cytochrome oxidases, and thereby on oxygen utilization by these oxidases was tested by using methylene blue as an oxygen probe. In the presence of oxygen, methylene blue becomes oxidized to cause a liquid solution to turn blue. However, in an actively respiring bacterial culture where oxygen is consumed, methylene blue is not readily oxidized and hence it decolourises. The effect of SCR0911 on bacterial oxygen consumption was observed through its effect on methylene blue decolourisation.

Thioridazine (THZ) is known to directly affect respiration, and is used as a positive control in the methylene blue assay.[36] As visualized in Figure 6A, 2.5x MIC_{50} of SCR0911 inhibited methylene blue decolourisation, indicating that oxygen consumption was inhibited, similar to the positive control of THZ. This is reflected in the calculated decolourization percentage which was 0% at 2.5x MIC_{50} of SCR0911 (Fig 6B). Similar observations were made at 5x and 10x MIC_{50} of SCR0911 (Fig 6A). However, the solubility of SCR0911 at

these higher concentrations could have affected the absorbance readings of the methylene blue decolourisation in the samples and consequently caused aberrant calculated decolourization percentage values (Fig 6B). Collectively, these results establish that SCR0911 effectively affects the electron flow from menaquinol to the final electron acceptor oxygen within the cyt-*bcc*-*aa3* super-complex, providing hints to its binding target.

Interestingly, in case of the cytochrome *bcc* inhibitor Q203, which does not cause oxygen consumption inhibition in *Mtb* H37Rv strains, it has been predicted that Q203 binds to the Q_o-site with the binding region spanning from residues $_{307}$DFYMMWTEGLA$_{317}$.[11, 15] Out of the four *Mtb cyt-bc1*-SCR0911 complex configurations studied, only the first major binding site is closer to the Q_o-site and it is behind the Q_o-site. Therefore, it can be speculated that SCR0911 might have a different mode of action than Q203.

Since BDQ inhibition in the F-ATP synthase has been shown to work also as an uncoupler, and to test whether SCR0911 might reveal any undefined uncoupling effects, an ATP-driving proton translocation assay was carried out. At the start of the experiment, 9-amino-6-chloro-2-methoxyacridine (ACMA) was added to IMVs, which were prepared according to Kamariah et al. (2019), and fluorescence was observed.[35] With the addition of NADH, an electron transfer was initiated, followed by the formation of a proton gradient, which caused quenching of the fluorescence dye and reduction in intensity. When SCR0911 was added, the fluoresence changed only weakly, while when the protonophore SF6847 was used as a positive control, the pH gradient collapsed, indicating that SCR0911 is not an uncoupler (Fig. 7).

CONCLUSION

One of the strategies to discover new drugs is to repurpose existing compounds, thus reducing the cost and time of drug discovery and / or development. The synthesis and

biological testing of SCR0911 revealed that the antimalarial compound is a potent inhibitor of *M. smegmatis* and *M. bovis* BCG growth. Effective reduction of ATP synthesis, in both the mycobacterial IMVs and whole cell assays, demonstrated that SCR0911 disrupts oxidative phosphorylation of mycobacteria. The use of the electron donor succinate excluded NADH-dehydrogenase and the succinate-dehydrogenase as direct target, while the loss of SCR0911 potency in the *M. smegmatis* Δ*bcc* mutant strain supported that cytochrome *bcc* is the direct target of the compound. The reduction in oxygen consumption confirms the interruption of electron flow within the cyt-*bcc*-*aa3* super-complex. The docking studies presented, confirm the whole cell-based and *in vitro* studies and described the ability of SCR0911 to bind to the Q_i site of the mycobacterial cyt-*bcc*, similar to the region modelled for the compound inside the *P. falciparum* oxidase.[32] Despite having a similar binding region, the interacting residues differ vastly, indicating SCR0911 adopts a different conformation in the mycobacterial cyt-*bcc* complex, and that SCR0911 is surrounded by mycobacterial specific residues (Supplementary Figure 1; Fig. 2E). Opening the door for the design and structure-activity relationship studies to improve the potency of new mycobacteria specific SCR0911 analogs as well as to avoid toxicity in compounds targeting the human cytochrome bc_1.

MATERIALS AND METHODS

Homology modelling of *Mtb* cyt-*bcc*

The *Mtb* cyt-*bcc*-model was generated using homology modelling within the SWISS-MODEL server.[37] The program accepts the target amino acid sequence an. searches for evolutionary related protein structures against the template library SMTL using BLAST and HHblits.[38, 39] The templates were then ranked based on global model quality estimate (GMQE) and quaternary structure quality estimate (QSQE). Finally, the 3D model of the *Mtb* cyt-*bcc* was generated with the *M. smegmatis* EM structure (PDB ID: 6ADQ) as a template and using

ProMod3 modelling engine that first transfers conserved atom coordinates defined by the target-template alignment.[21] Afterwards, insertions/deletions were constructed using loop modelling. The heme groups were manually modelled into the *Mtb* complex, the individual subunits were assembled to generate a monomer, and a dimer model was created based on the *M. smegmatis* EM structure (PDB ID: 6ADQ).

Docking studies of SCR0911 with *Mtb* cyt-*bcc*

Docking studies were carried out for SCR0911 with the homology model of *Mtb* cyt-*bcc*. The three-dimensional structure of SCR0911 was retrieved from the crystal structure of bovine cytochrome bc_1 complex (PDB ID: 5OKD).[32] The SCR0911 was docked into the model of *Mtb* cyt-*bcc* -using AutoDock 4.2.[40] Autodock is a computational docking program which is based on the Lamarckian Genetic Algorithm search method and an empirical free energy scoring function. The free-energy scoring function is based on a linear regression analysis, the AMBER force field, and a larger set of diverse protein-ligand complexes with known inhibition constants. The program consists of two parts, AutoDock for docking of the ligand to a set of grids describing the target protein; and AutoGrid for pre-calculating these grids. The 100 protein-ligand complex models scored based on the weighted sum of steric interactions, hydrophobic interaction, and hydrogen bonding were analyzed. The complex configurations were then clustered based on the results by conformational similarity, visualizing conformations, visualizing interactions between ligands and proteins, and visualizing the affinity potentials created by AutoGrid. The best model with the highest score from each cluster was selected for further analysis. The model was visualized using PyMOL, and the interactions profile was represented using LIGPLOT.[41, 42]

Synthesis of SCR0911

The synthesis of SCR0911 was carried out following the procedure by Charoensutthivarakul et al. (2015) with several modifications to the synthesis scheme.[30]

4,4,5,5-Tetramethyl-2-(4-(trifluoromethoxy)phenyl)-1,3,2-dioxaborolane (2)[43]

A mixture of bis(pinacolato)diboron (0.658 g, 2.59 mmol), compound **7** (0.500 g, 2.07 mmol), potassium acetate (0.311 g, 3.17 mmol) and Pd(dppf)Cl_2 in tetrahydrofuran (THF) (5 ml) was heated at reflux overnight under nitrogen before cooling to room temperature. Ethyl acetate (15 ml) was added, and the mixture was filtered through a pad of Celite (R). The filtrate was washed with water (10 ml x 2) and concentrated in *vacuo*. The residue was purified by flash chromatography (10 – 25% ethyl acetate:hexane) to afford the title compound as a colourless solid (0.39 g, 1.35 mmol, 65%). δ_H (400 MHz, $CDCl_3$) 7.84 (d, J = 8.6 Hz, 2H), 7.20 (d, J = 8.7 Hz, 2H), 1.34 (s, 12H) ppm.[44]

5-Bromo-*N*-methoxy-*N*-methylnicotinamide (9)

4- (Dimethylamino)pyridine (DMAP) (0.242 g, 1.98 mmol) and *N*-(3-dimethylaminopropyl)-*N*'-ethylcarbodiimide hydrochloride (EDCI) (2.85 g, 14.9 mmol) were added to a solution of compound **8** (2 g, 9.90 mmol) and *N, O*-dimethylhydroxylamine hydrochloride (1.45 g, 14.9 mol) in dichloromethane (36 ml). The mixture was placed under nitrogen and triethylamine (2.0 ml, 14.8 mmol) was added dropwise. The mixture was stirred overnight at room temperature. Water (50 ml) was added, followed by extraction with dichloromethane (3 x 30 ml). The combined organic layers were washed with brine (50 ml), dried over anhydrous Na_2SO_4 and concentrated in *vacuo*. The residue was purified by flash chromatography (50% ethyl acetate: hexane) to afford the title compound as a yellow solid (2.10 g, 8.55 mmol, 86%). δ_H (400 MHz, $CDCl_3$) 8.87 (d, J = 1.8 Hz, 1H), 8.75 (d, J = 2.3 Hz, 1H)8.17 (t, J = 2.0 Hz, 1H), 3.57 (s, 3H), 3.39 (s, 3H) ppm.[45]

1-(5-Bromopyridin-3-yl)propan-1-one (3)[46]

Ethyl magnesium bromide (34.2 mmol, 4.0 eq) was added dropwise to a solution of amide **9** (2.11 g, 8.61 mmol) in THF (85 ml) under nitrogen at 0 °C. The solution was stirred for 30 minutes at 0 °C, then quenched with saturated NH_4Cl (50 ml) before extraction with diethyl ether (3 x 50 ml). The combined organic layers were washed with brine (50 ml), dried over $MgSO_4$ and concentrated in *vacuo*. The residue was purified by flash chromatography (50% ethyl acetate: hexane) to afford the title compound as a yellow solid (0.655 g, 3.06 mmol, 36%). δ_H (400 MHz, $CDCl_3$) 9.07 (d, J = 1.7 Hz, 1H), 8.84 (d, J = 2.1 Hz, 1H), 8.40 – 8.33 (m, 1H), 3.01 (q, J = 7.2 Hz, 2H), 1.25 (t, J = 7.2 Hz, 3H) ppm; HRMS (EI) 213.9849 $[M+H]^+$.

1-(5-(4-(Trifluoromethoxy)phenyl)pyridin-3-yl)propan-1-one (1)[30]

Compound **2** (0.321 g, 1.12 mmol) was added to a stirred solution of compound **3** (0.218 g, 1.02 mmol), $Pd(dppf)Cl_2$ (0.059 g, 0.081 mmol) and potassium carbonate (0.463 g, 3.37 mmol) in THF: H_2O (16 ml: 6.4ml) under nitrogen. The mixture was heated at reflux overnight before cooling to room temperature. Water (10 ml) was added, and the organic layer was extracted with ethyl acetate (3 x 15 ml). The combined organic layers were washed with brine, dried over $MgSO_4$ and concentrated in *vacuo*. The residue was purified by flash chromatography (30% ethyl acetate: hexane) to afford the title compound as a yellow solid (0.284 g, 0.96 mmol, 47%). δ_H (400 MHz, $CDCl_3$) 9.16 (d, *J* = 2.0 Hz, 1H), 8.98 (d, *J* = 2.3 Hz, 1H), 8.40 (t, *J* = 2.2 Hz, 1H), 7.67 – 7.62 (m, 2H), 7.36 (d, *J* = 7.9 Hz, 2H), 3.09 (q, *J* = 7.2 Hz, 2H), 1.29 (t, *J* = 7.2 Hz, 3H) ppm.[30]

2-Iodo-5-methoxyaniline (11)[47]

N-Iodosuccinimide (0.995 g, 4.06 mmol) was added to a solution of 3-methoxyaniline (0.46 ml, 4.06 mmol) in dichloromethane (100 ml) and acetic acid (0.25 ml, 4.25 mmol). The mixture was stirred overnight at room temperature. Aqueous $NaHCO_3$ (100 ml) was added, and the organic layer was extracted with ethyl acetate (3 x 40 ml). The combined organic

layers were washed with brine, dried over $MgSO_4$ and concentrated in *vacuo*. The residue was purified by flash chromatography (ethyl acetate: hexane) to afford the title compound as a brown oil (0.530 g, 2.13 mmol, 52%). δ_H (400 MHz, $CDCl_3$) 7.48 (d, J = 8.7 Hz, 1H), 6.33 (d, J = 2.8 Hz, 1H), 6.14 (dd, J = 8.7, 2.8 Hz, 1H), 4.07 (s, 2H), 3.74 (s, 3H) ppm.[47]

Methyl 2-amino-4-methoxybenzoate (12)

A solution of compound **11** (0.123 g, 0.440 mmol), and $Pd(dppf)Cl_2$ (0.0129 g, 0.0176 mmol) in methanol (2 ml) was placed under an atmosphere of carbon monoxide (balloon). Triethylamine (0.06 ml, 0.474 mmol) was added to the reaction mixture and carbon monoxide was bubbled through the mixture for 30 seconds. The mixture was heated at reflux overnight. Ethyl acetate (10 ml) was added and the mixture was filtered through a pad of Celite(R), before concentration in *vacuo*. The residue was purified by flash chromatography (10 – 25% ethyl acetate:hexane) to afford the title compound as a brown solid (0.07 g, 0.384 mmol, 87%). δ_H (400 MHz, $CDCl_3$) 7.79 (d, J = 9.0 Hz, 1H), 6.23 (dd, J = 9.0, 2.5 Hz, 1H), 6.11 (d, J = 2.5 Hz, 1H), 3.84 (s, 3H), 3.79 (s, 3H) ppm.[48]

2-Amino-4-methoxybenzoic acid (6)

Lithium hydroxide (0.032 g, 0.77 mmol) was added to a solution of compound **12** (0.070 g, 0.38 mmol) in THF:H_2O (1 ml :1ml). The mixture was heated at reflux for 5 hours. The mixture was allowed to cool to room temperature and the aqueous layer was collected. 2 M HCl was added dropwise until the pH reached to 3. The aqueous solution was extracted with EtOAc (3 x 10 ml) before concentrating in *vacuo* to afford a white solid (0.057 g, 0.343 mmol, 89%). δ_H (400 MHz, $(CD_3)_2SO$) 7.60 (d, *J* = 8.9 Hz, 1H), 6.22 (d, *J* = 2.5 Hz, 1H), 6.09 (dd, *J* = 8.9, 2.5 Hz, 1H), 3.71 (s, 3H) ppm.[49]

2-(4,4-Dimethyl-4,5-dihydrooxazol-2-yl)-5-methoxyaniline (4)

Triphenylphosphine (0.474 g, 1.81 mmol), triethylamine (0.25 ml, 1.81 mmol), CBr_4 (0.599 g, 1.81 mmol), aromatic acid **6** (0.100 g, 0.602 mmol), and 2-amino-2-methylpropan-

1-ol (0.07 ml, 0.704 mmol) in toluene (3 ml) was stirred under nitrogen for 20 minutes at room temperature before being heated at 90 °C overnight. The solvent was evaporated under reduced pressure, and the residue was diluted with diethyl ether and filtered. The residual solid was washed with ether three times. The filtrate was concentrated in *vacuo* and purified by flash chromatography (5% -20% ethyl acetate:hexane) to afford the title compound as a white solid (0.0256 g, 0.116 mmol, 19%). δ_H (400 MHz, $CDCl_3$) δ 7.59 (d, *J* = 8.8 Hz, 1H), 6.83 (s, 1H), 6.24 (dd, *J* = 8.8, 2.5 Hz, 1H), 6.17 (d, *J* = 2.5 Hz, 1H), 3.96 (s, 2H), 3.78 (s, 3H), 1.35 (s, 6H) ppm.[30]

7-methoxy-3-methyl-2-(5-(4-(trifluoromethoxy)phenyl)pyridin-3-yl)quinolin-4(1H)-one (SCR0911)

Trifluoromethane sulfonic acid (0.006 ml, 0.067 mmol) was added to a solution of oxazoline **1** (0.0806 g, 0.366 mmol) and ketone **4** (0.983, 0.33 mmol) in dry n-butanol (5.5 ml). The mixture was heated at reflux for 24 hours. Saturated sodium carbonate solution (10 ml) was added. The aqueous solution was extracted with ethyl acetate (3 x 15 ml) and combined organic layers were washed with brine (50 ml), dried over $MgSO_4$ and concentrated in *vacuo*. The residue was purified by flash chromatography (5 – 20% ethyl acetate: hexane) to afford the title compound as a brown solid (0.062 g, 0.155 mmol, 42%). δH (400 MHz, DMSO) 11.56 (s, 1H), 9.10 (d, J = 2.2 Hz, 1H), 8.79 (d, J = 2.0 Hz, 1H), 8.34 (t, J = 2.2 Hz, 1H), 8.03 (dd, J = 18.1, 8.9 Hz, 4H), 7.54 (d, J = 7.9 Hz, 3H), 1.94 (s, 3H) ppm; HRMS (EI) 427.1288 $[M+H]^+$.[30]

Minimum inhibitory concentration determination

The growth inhibition dose-response assay was carried out using the broth microdilution method, as described previously.[34, 50] Briefly, clear 96-well flat-bottom Costar cell culture plates (Corning) were filled with 100 µl of complete 7H9 medium supplemented with

albumin–dextrose–catalase (ADC), without glycerol, in each well. Each compound was added to the first well in each row to create two times the desired highest final concentration. Subsequently, a 10-point 2-fold serial dilution was carried out starting from the first well in each row. *M. bovis* bacillus Calmette–Guérin (BCG), *M. smegmatis mc²155*- and the isogenic *M. smegmatis* strain ZCW111 Δ*bcc* mutant used for the assays were grown to mid-log phase in complete 7H9 medium. The cells were washed with glycerol-free 7H9 media and subsequently diluted to an OD_{600} of 0.1 and 0.01, respectively. 100 µl of the diluted culture was added to each well to create a final OD_{600} of 0.05 and 0.005 for *M. smegmatis* and *M. bovis* Bacillus Calmette-Guérin (BCG) respectively, in all wells. For *M. smegmatis* strains, the plates were incubated at 37 °C on an orbital shaker set at 180 rpm for 24 hours. For *M. bovis* BCG strains, the plates were incubated at 37 °C without shaking for 7 days. At the end of the incubation period, the culture in all wells was manually resuspended, and the OD_{600} was read using a TECAN Infinite Pro 200 plate reader. The MIC_{50} reported represents the concentration that inhibits 50% of growth compared to the untreated culture.

Markerless mutant construction of the Δ*bcc* mutant

In brief, to generate the *M. smegmatis* Δ*bcc* mutant, two homologous regions either side of the target gene (primers ZW1, ZW2, ZW3, ZW4) (Supplementary Table 1) were cloned into pX33 using NEBuilder® HiFi DNA Assembly (NEB) as per the manufacturer's instructions with the SpeI restriction enzyme (NEB). The pX33 constructs with homologous regions (pX33qcr) were electroporated into *M. smegmatis* mc^2155 and grown at 28°C to ensure permissibility of the pX33 temperature-sensitive plasmid. Confirmation of the plasmid transformation was achieved by treating colonies with 250 mM catechol. Colonies containing the plasmid turn yellow owing to the catechol dioxygenase produced by pX33. Following plasmid confirmation, the cells were grown on liquid media at 28°C and then plated at 40°C

to select integration events based on the homology of the gene flanking regions. Integrants were confirmed through catechol screening (as above). Integrants were spread-plated on sucrose (10% w/v) containing media to force recombination to either the wildtype genotype or the markerless deletion mutant.[51] The Δ*bcc* mutant was confirmed using PCR (primer pair, ZW5, ZW6) and whole-genome sequencing (WGS) and aligned using to wildtype to confirm that the gene was deleted using geneious (Supplementary Figure S2A and S2B). The resulting *bcc* deletion mutant was designated ZCW111.

Complementation of *M. smegmatis* strain ZCW111 Δ*bcc* mutant

The construct for the strain ZCW111 Δ*bcc* complementation was made using the pMV361 vector backbone. The *qcrCAB* genes were amplified using LH1 and LH2 primer pairs (Supplementary Table 1). The respective product was then digested with HindIII and HpaI restriction enzymes before ligation into the pMV361 vector. The resulting plasmid is termed pMV361qcr. Functionality of the pMV361qcr vector for complementation was tested through the growth of Δ*bcc* and Δ*bcc* + pMV361qcr on HdeB agar with 50 mM succinate as the sole carbon and energy source (Supplementary Figure S2C).

DNA manipulation and cloning

All molecular biology techniques were carried out according to standard procedures. All restriction enzymes and DNA modifying enzymes used were from New England Biolabs (NEB) and were in their appropriate buffers. All constructs were confirmed using either PCR or restriction digests followed by sequencing. PCR for construct creation was done using Thermo Fisher Phusion polymerase following the recommended conditions with appropriate annealing temperatures and extension time.

Intracellular ATP synthesis assay

The intracellular ATP synthesis assay was carried out using the broth microdilution method as described previously, using the BacTiter-Glo™ Microbial Cell Viability Assay kit (Promega) to quantify the intracellular ATP.[34, 50, 52] Clear 96-well flat-bottom Costar cell culture plates (Corning) were filled with 100 µl of complete 7H9 medium supplemented with ADC, in each well. Each compound was added to the first well in each row to create two times the desired highest final concentration. Subsequently, a 10-point 2-fold serial dilution was carried out starting from the first well in each row. *M. bovis* BCG stains were grown in complete 7H9 medium to mid-log phase and subsequently diluted to an OD_{600} of 0.1. 100 µl of the diluted culture was added to each well to create a final OD_{600} of 0.05 in all wells. The plates were incubated at 37 °C on an orbital shaker set at 110 rpm for 24 hours. 50 µl of samples (total culture) were mixed with an equal volume of freshly prepared BacTiter-Glo™ reagent in white flat bottomed 96 well plates (Corning) and lysis was carried out for 10 min at room temperature with shaking at an amplitude of 3 mm inside the TECAN Infinite Pro 200 plate reader. Emitted luminescence was displayed as relative light units (RLU).

Production of *M. smegmatis* inverted membrane vesicles (IMVs)

Preparation of the IMVs were carried out as previously described by Hotra *et al.*, 2016 and Kamariah *et al.*, 2019.[53] [35]

ATP synthesis assay using IMVs

The ATP synthesis assay was quantified with the CellTiter-Glo® Luminescent Cell Viability Assay kit (Promega). ATP synthesis measurement was carried out on white flat-bottomed 96-well microtiter plates (Corning). 2.5 µl of compounds at varying concentration was spotted on the individual wells. This was followed by the addition of 25 µl of PMVs or

IMVs (5 μg/ml) and 25 μL of assay buffer (50 mm MOPS, pH 7.5, 10 mM $MgCl_2$), containing 10 μM ADP, 250 μM Pi and 1 mM NADH. The plates were incubated at room temperature for 30 minutes before the addition of 25 μl of CellTiter-Glo® reagent. The plates were incubated for another 10 min in the dark at room temperature. The luminescence was measured by a TECAN Infinite Pro 200 plate reader.

Oxygen consumption assay

Oxygen comsumption assay was carried out using methylene blue as previously described by Li *et al.*, 2017.[54].The percentage of methylene blue decolourization in the samples was determined using the methylene blue absorbance readings and the equation below as described previously by Benetoli et al., where A_o represents the absorbance of the 7H9 sample, while A_s represents the absorbance of the sample of interest [55].

$$D\% = \frac{A_o - A_s}{A_o} \times 100$$

Assay for ATP-driven proton translocation

ATP-driven proton translocation of plasma membrane vesicles of *M. smegmatis* were measured on the basis of a decrease in ACMA fluorescence using a Cary Eclipse fluorescence spectrophotometer (Varian Inc., Palo Alto, CA) as described previously.[56] IMVs or PMVs (0.18 mg/mL) were pre-incubated at 37 °C in 10 mM HEPES/KOH (pH 7.5), 100 mM KCl, 5 mM $MgCl_2$ containing 2 μM ACMA, 50 μM ADP and 5 mM Pi. A baseline was obtained by monitoring for 2 min. The reaction was started by adding 0.5 mM NADH or succinate as electron donors. After approximately another 2 to 4 min when the florescence intensity was quenched completely, 15 μM of the test compound was added. After another 2 minutes, the proton gradient was collapsed completely via the addition of 2 μM of the

uncoupler SF6847 (Alexis Corporation, Lausen, Switzerland). The excitation and emission wavelengths were 410 and 480 nm, respectively.

Acknowledgements:

This research was supported by the National Research Foundation (NRF) Singapore, NRF Competitive Research Programme (CRP), Grant Award Number NRF–CRP18–2017–01). C. S. M. Sherilyn is grateful to receive an NTU research scholarship at Nanyang Technological University Singapore.

Conflict of interest: The authors declare that they have no conflicts of interest with the contents of this article.

Author contributions: C.S.M.S., M.S.S.M., G.M.C., T.D., K.P, and G.G. conceived and designed the experiments. C.S.M.S., M.S.S.M., J.P.S., Z.C.W., and L.K.H. performed the experiments and analyzed the data. C.S.M.S., M.S.S.M., and G.G. wrote the paper with contribution from other authors.

REFERENCES

1. Gulland, A., World leaders heed Macron's call and pledge $14bn to fight killer diseases. *The Telegraph* 10 October 2019, 2019.
2. World Health Organisation. Global tuberculosis report 2019. https://www.who.int/tb/publications/global_report/en/.
3. Blumberg, H. M.; Ernst, J. D., The Challenge of Latent TB Infection. *JAMA* **2016,** *316* (9), 931-933.
4. Joshi, J. M., Tuberculosis chemotherapy in the 21(st) century: Back to the basics. *Lung India : Official Organ of Indian Chest Society* **2011,** *28* (3), 193-200.
5. Bhat, Z. S.; Rather, M. A.; Maqbool, M.; Ahmad, Z., Drug targets exploited in Mycobacterium tuberculosis: Pitfalls and promises on the horizon. *Biomedicine & Pharmacotherapy* **2018,** *103*, 1733-1747.
6. World Health Organisation. Global tuberculosis report 2015. http://apps.who.int/iris/handle/10665/191102.

7. Sacchettini, J. C.; Rubin, E. J.; Freundlich, J. S., Drugs versus bugs: in pursuit of the persistent predator Mycobacterium tuberculosis. *Nat Rev Micro* **2008,** *6* (1), 41-52.
8. Almeida Da Silva, P. E.; Palomino, J. C., Molecular basis and mechanisms of drug resistance in Mycobacterium tuberculosis: classical and new drugs. *Journal of Antimicrobial Chemotherapy* **2011,** *66* (7), 1417-1430.
9. Frank, D. J.; Horne, D. J.; Dutta, N. K.; Shaku, M. T.; Madensein, R.; Hawn, T. R.; Steyn, A. J. C.; Karakousis, P. C.; Kana, B. D.; Meintjes, G.; Laughon, B.; Tanvir, Z., Remembering the Host in Tuberculosis Drug Development. *The Journal of Infectious Diseases* **2018,** *219* (10), 1518-1524.
10. Barry, V. C.; Belton, J. G.; Conalty, M. L.; Denneny, J. M.; Edward, D. W.; O'Sullivan, J. F.; Twomey, D.; Winder, F., A New Series of Phenazines (Rimino-Compounds) With High Antituberculosis Activity. *Nature* **1957,** *179* (4568), 1013-1015.
11. Pethe, K.; Bifani, P.; Jang, J.; Kang, S.; Park, S.; Ahn, S.; Jiricek, J.; Jung, J.; Jeon, H. K.; Cechetto, J., Discovery of Q203, a potent clinical candidate for the treatment of tuberculosis. *Nature medicine* **2013,** *19* (9), 1157.
12. Andries, K.; Verhasselt, P.; Guillemont, J.; Göhlmann, H. W. H.; Neefs, J.-M.; Winkler, H.; Van Gestel, J.; Timmerman, P.; Zhu, M.; Lee, E.; Williams, P.; de Chaffoy, D.; Huitric, E.; Hoffner, S.; Cambau, E.; Truffot-Pernot, C.; Lounis, N.; Jarlier, V., A Diarylquinoline Drug Active on the ATP Synthase of Mycobacterium tuberculosis. *Science* **2005,** *307* (5707), 223-227.
13. (FDA), F. A. D. A. FDA approves new drug for treatment-resistant forms of tuberculosis that affects the lungs. https://www.fda.gov/news-events/press-announcements/fda-approves-new-drug-treatment-resistant-forms-tuberculosis-affects-lungs.
14. Matsoso, L. G.; Kana, B. D.; Crellin, P. K.; Lea-Smith, D. J.; Pelosi, A.; Powell, D.; Dawes, S. S.; Rubin, H.; Coppel, R. L.; Mizrahi, V., Function of the cytochrome bc1-aa3 branch of the respiratory network in mycobacteria and network adaptation occurring in response to its disruption. *Journal of bacteriology* **2005,** *187* (18), 6300-6308.
15. Kalia, N. P.; Hasenoehrl, E. J.; Ab Rahman, N. B.; Koh, V. H.; Ang, M. L.; Sajorda, D. R.; Hards, K.; Grüber, G.; Alonso, S.; Cook, G. M., Exploiting the synthetic lethality between terminal respiratory oxidases to kill Mycobacterium tuberculosis and clear host infection. *Proceedings of the National Academy of Sciences* **2017,** *114* (28), 7426-7431.
16. Kalia, N. P.; Shi Lee, B.; Ab Rahman, N. B.; Moraski, G. C.; Miller, M. J.; Pethe, K., Carbon metabolism modulates the efficacy of drugs targeting the cytochrome bc(1):aa(3) in Mycobacterium tuberculosis. *Scientific Reports* **2019,** *9* (1), 8608-8608.
17. Beites, T.; O'Brien, K.; Tiwari, D.; Engelhart, C. A.; Walters, S.; Andrews, J.; Yang, H.-J.; Sutphen, M. L.; Weiner, D. M.; Dayao, E. K.; Zimmerman, M.; Prideaux, B.; Desai, P. V.; Masquelin, T.; Via, L. E.; Dartois, V.; Boshoff, H. I.; Barry, C. E.; Ehrt, S.; Schnappinger, D., Plasticity of the Mycobacterium tuberculosis respiratory chain and its impact on tuberculosis drug development. *Nature Communications* **2019,** *10* (1), 4970.
18. Moosa, A.; Lamprecht, D. A.; Arora, K.; Barry, C. E.; Boshoff, H. I. M.; Ioerger, T. R.; Steyn, A. J. C.; Mizrahi, V.; Warner, D. F., Susceptibility of Mycobacterium tuberculosis Cytochrome bd Oxidase Mutants to Compounds Targeting the Terminal Respiratory Oxidase, Cytochrome c. *Antimicrobial Agents and Chemotherapy* **2017,** *61* (10), e01338-17.
19. Cook, G. M.; Greening, C.; Hards, K.; Berney, M., Chapter One - Energetics of Pathogenic Bacteria and Opportunities for Drug Development. In *Advances in Microbial Physiology*, Poole, R. K., Ed. Academic Press: 2014; Vol. 65, pp 1-62.
20. Wiseman, B.; Nitharwal, R. G.; Fedotovskaya, O.; Schäfer, J.; Guo, H.; Kuang, Q.; Benlekbir, S.; Sjöstrand, D.; Ädelroth, P.; Rubinstein, J. L.; Brzezinski, P.; Högbom, M., Structure of a functional obligate complex III2IV2 respiratory supercomplex from

Mycobacterium smegmatis. *Nature Structural & Molecular Biology* **2018,** *25* (12), 1128-1136.
21. Gong, H.; Li, J.; Xu, A.; Tang, Y.; Ji, W.; Gao, R.; Wang, S.; Yu, L.; Tian, C.; Li, J.; Yen, H.-Y.; Man Lam, S.; Shui, G.; Yang, X.; Sun, Y.; Li, X.; Jia, M.; Yang, C.; Jiang, B.; Lou, Z.; Robinson, C. V.; Wong, L.-L.; Guddat, L. W.; Sun, F.; Wang, Q.; Rao, Z., An electron transfer path connects subunits of a mycobacterial respiratory supercomplex. *Science* **2018,** *362* (6418), eaat8923.
22. Kana, B. D.; Weinstein, E. A.; Avarbock, D.; Dawes, S. S.; Rubin, H.; Mizrahi, V., Characterization of the *cydAB*-encoded cytochrome *bd* oxidase from *Mycobacterium smegmatis*. *J. Bacteriol.* **2001,** *183* (24), 7076-86.
23. Black, P. A.; Warren, R. M.; Louw, G. E.; van Helden, P. D.; Victor, T. C.; Kana, B. D., Energy metabolism and drug efflux in Mycobacterium tuberculosis. *Antimicrobial agents and chemotherapy* **2014**, AAC. 02293-13.
24. Matta, S. K.; Kumar, D., Hypoxia and classical activation limits Mycobacterium tuberculosis survival by Akt-dependent glycolytic shift in macrophages. *Cell Death Discov* **2016,** *2*, 16022-16022.
25. Giuffrè, A.; Borisov, V. B.; Arese, M.; Sarti, P.; Forte, E., Cytochrome bd oxidase and bacterial tolerance to oxidative and nitrosative stress. *Biochimica et Biophysica Acta (BBA) - Bioenergetics* **2014,** *1837* (7), 1178-1187.
26. Bald, D.; Villellas, C.; Lu, P.; Koul, A., Targeting Energy Metabolism in Mycobacterium tuberculosis, a New Paradigm in Antimycobacterial Drug Discovery. *MBio* **2017,** *8* (2), e00272-17.
27. Nzila, A.; Ma, Z.; Chibale, K., Drug repositioning in the treatment of malaria and TB. *Future Medicinal Chemistry* **2011,** *3* (11), 1413-1426.
28. Padayatchi, N.; Gopal, M.; Naidoo, R.; Werner, L.; Naidoo, K.; Master, I.; O'donnell, M., Clofazimine in the treatment of extensively drug-resistant tuberculosis with HIV coinfection in South Africa: a retrospective cohort study. *J. Antimicrob. Chemother.* **2014,** *69* (11), 3103-3107.
29. Kuo, M. R.; Morbidoni, H. R.; Alland, D.; Sneddon, S. F.; Gourlie, B. B.; Staveski, M. M.; Leonard, M.; Gregory, J. S.; Janjigian, A. D.; Yee, C., Targeting tuberculosis and malaria through inhibition of enoyl reductase compound activity and structural data. *Journal of Biological Chemistry* **2003,** *278* (23), 20851-20859.
30. Charoensutthivarakul, S.; Hong, W. D.; Leung, S. C.; Gibbons, P. D.; Bedingfield, P. T.; Nixon, G. L.; Lawrenson, A. S.; Berry, N. G.; Ward, S. A.; Biagini, G. A., 2-Pyridylquinolone antimalarials with improved antimalarial activity and physicochemical properties. *MedChemComm* **2015,** *6* (7), 1252-1259.
31. Capper, M. J.; O'Neill, P. M.; Fisher, N.; Strange, R. W.; Moss, D.; Ward, S. A.; Berry, N. G.; Lawrenson, A. S.; Hasnain, S. S.; Biagini, G. A.; Antonyuk, S. V., Antimalarial 4(1H)-pyridones bind to the Qi site of cytochrome bc1. *Proceedings of the National Academy of Sciences* **2015,** *112* (3), 755-760.
32. Amporndanai, K.; Johnson, R. M.; O'Neill, P. M.; Fishwick, C. W.; Jamson, A. H.; Rawson, S.; Muench, S. P.; Hasnain, S. S.; Antonyuk, S. V., X-ray and cryo-EM structures of inhibitor-bound cytochrome bc1 complexes for structure-based drug discovery. *IUCrJ* **2018,** *5* (2), 200-210.
33. Kundu, S.; Biukovic, G.; Grüber, G.; Dick, T., Bedaquiline Targets the ε Subunit of Mycobacterial F-ATP Synthase. *Antimicrobial Agents and Chemotherapy* **2016,** *60* (11), 6977-6979.
34. Moreira, W.; Aziz, D. B.; Dick, T., Boromycin Kills Mycobacterial Persisters without Detectable Resistance. *Frontiers in Microbiology* **2016,** *7* (199).

35. Kamariah, N.; Huber, R. G.; Nartey, W.; Bhushan, S.; Bond, P. J.; Grüber, G., Structure and subunit arrangement of Mycobacterial F1FO ATP synthase and novel features of the unique mycobacterial subunit δ. *Journal of Structural Biology* **2019,** *207* (2), 199-208.
36. Boshoff, H. I.; Myers, T. G.; Copp, B. R.; McNeil, M. R.; Wilson, M. A.; Barry, C. E., The transcriptional responses of Mycobacterium tuberculosis to inhibitors of metabolism novel insights into drug mechanisms of action. *Journal of Biological Chemistry* **2004,** *279* (38), 40174-40184.
37. Waterhouse, A.; Bertoni, M.; Bienert, S.; Studer, G.; Tauriello, G.; Gumienny, R.; Heer, F. T.; de Beer, T. A. P.; Rempfer, C.; Bordoli, L.; Lepore, R.; Schwede, T., SWISS-MODEL: homology modelling of protein structures and complexes. *Nucleic acids research* **2018,** *46* (W1), W296-W303.
38. Camacho, C.; Coulouris, G.; Avagyan, V.; Ma, N.; Papadopoulos, J.; Bealer, K.; Madden, T. L., BLAST+: architecture and applications. *BMC bioinformatics* **2009,** *10*, 421-421.
39. Remmert, M.; Biegert, A.; Hauser, A.; Söding, J., HHblits: lightning-fast iterative protein sequence searching by HMM-HMM alignment. *Nature Methods* **2012,** *9* (2), 173-175.
40. Morris, G. M.; Huey, R.; Lindstrom, W.; Sanner, M. F.; Belew, R. K.; Goodsell, D. S.; Olson, A. J., AutoDock4 and AutoDockTools4: Automated docking with selective receptor flexibility. *J Comput Chem* **2009,** *30* (16), 2785-2791.
41. DeLano, W. L., PyMOL. 2002.
42. Wallace, A. C.; Laskowski, R. A.; Thornton, J. M., LIGPLOT: a program to generate schematic diagrams of protein-ligand interactions. *Protein Engineering, Design and Selection* **1995,** *8* (2), 127-134.
43. Zhai, J.; Pan, T.; Zhu, J.; Xu, Y.; Chen, J.; Xie, Y.; Qin, Y., Boronic acid functionalized boron dipyrromethene fluorescent probes: preparation, characterization, and saccharides sensing applications. *Analytical chemistry* **2012,** *84* (23), 10214-10220.
44. Zhao, C.-J.; Xue, D.; Jia, Z.-H.; Wang, C.; Xiao, J., Methanol-promoted Borylation of Arylamines: A simple and green synthetic method to Arylboronic acids and Arylboronates. *Synlett* **2014,** *25* (11), 1577-1584.
45. Tomoaki, M.; Kenichi, K.; Satomi, N.; Naoto, O.; Yumiko, F.; Takashi, W.; Hideki, F.; Kunio, A.; Keiichi, A. NOVEL AZALIDE AND AZALACTAM DERIVATIVES AND PROCESS FOR THE PRODUCTION OF THE SAME. 2004/08/20/Application date, 2004.
46. Paterson, I.; neÈ Doughty, V. A. S.; McLeod, M. D.; Trieselmann, T., Stereocontrolled total synthesis of (+)-concanamycin F: the strategic use of boron-mediated aldol reactions of chiral ketones. *Tetrahedron* **2011,** *67* (52), 10119-10128.
47. Shen, H.; Vollhardt, K. P. C., Remarkable Switch in the Regiochemistry of the Iodination of Anilines by N-Iodosuccinimide: Synthesis of 1, 2-Dichloro-3, 4-diiodobenzene. *Synlett* **2012,** *2012* (02), 208-214.
48. Hinsberger, S.; Hüsecken, K.; Groh, M.; Negri, M.; Haupenthal, J.; Hartmann, R. W., Discovery of Novel Bacterial RNA Polymerase Inhibitors: Pharmacophore-Based Virtual Screening and Hit Optimization. *Journal of Medicinal Chemistry* **2013,** *56* (21), 8332-8338.
49. Pavlidis, V. H.; Perry, P. J., The Synthesis of a Novel Series of Substituted 2-Phenyl-4H-3,1-benzoxazin-4-ones. *Synthetic Communications* **1994,** *24* (4), 533-548.
50. Gopal, P.; Dick, T., The new tuberculosis drug Perchlozone® shows cross-resistance with thiacetazone. *International Journal of Antimicrobial Agents* **2015,** *45* (4), 430-433.
51. Lu, X.; Williams, Z.; Hards, K.; Tang, J.; Cheung, C. Y.; Aung, H. L.; Wang, B.; Liu, Z.; Hu, X.; Lenaerts, A.; Woolhiser, L.; Hastings, C.; Zhang, X.; Wang, Z.; Rhee, K.; Ding, K.; Zhang, T.; Cook, G. M., Pyrazolo[1,5- *a*]pyridine inhibitor of the respiratory

cytochrome *bcc* complex for the treatment of drug-resistant tuberculosis. *ACS Infect. Dis.* **2019,** *5* (2), 239-249.
52. Gengenbacher, M.; Rao, S. P.; Pethe, K.; Dick, T., Nutrient-starved, non-replicating Mycobacterium tuberculosis requires respiration, ATP synthase and isocitrate lyase for maintenance of ATP homeostasis and viability. *Microbiology* **2010,** *156* (1), 81-87.
53. Hotra, A.; Suter, M.; Biuković, G.; Ragunathan, P.; Kundu, S.; Dick, T.; Grüber, G., Deletion of a unique loop in the mycobacterial F-ATP synthase γ subunit sheds light on its inhibitory role in ATP hydrolysis-driven H+ pumping. *The FEBS Journal* **2016,** *283* (10), 1947-1961.
54. Li, M.; Nyantakyi, S. A.; Gopal, P.; Aziz, D. B.; Dick, T.; Go, M.-L., Indolylalkyltriphenylphosphonium Analogues Are Membrane-Depolarizing Mycobactericidal Agents. *ACS Med Chem Lett* **2017,** *8* (11), 1165-1170.
55. Benetoli, L. O. d. B.; Cadorin, B. M.; Postiglione, C. d. S.; Souza, I. G. d.; Debacher, N. A., Effect of temperature on methylene blue decolorization in aqueous medium in electrical discharge plasma reactor. *Journal of the Brazilian Chemical Society* **2011,** *22* (9), 1669-1678.
56. Haagsma, A. C.; Driessen, N. N.; Hahn, M.-M.; Lill, H.; Bald, D., ATP synthase in slow- and fast-growing mycobacteria is active in ATP synthesis and blocked in ATP hydrolysis direction. *FEMS Microbiology Letters* **2010,** *313* (1), 68-74.

FIGURE LEGENDS

Figure 1. (A) Chemical structure of SCR0911.[30] The main difference lies in the position of the (trifluoromethoxy)benzene group in respect to the pyridine ring. (B) Sequence alignment of the cytochrome *b* of bovine, *P. falciparum*, *M. smegmatis*, *M. bovis*, and *M. tuberculosis*. The *orange boxes* indicate the residues that are significant in the *P. falciparum* homology model with the binding of the analog of SCR0911. The *green boxe*s indicate the residues that are significant in the bovine crystal structure with the binding of SCR0911. The numbers on the boxes refers to the residue number with respect to *P. falciparum.*

Figure 2. Docking studies of SCR0911 with *Mtb* cyt-*bcc* complex. (A) Cartoon representation of the 1st major docked complex configuration of *Mtb* cyt-*bcc* with SCR0911. Only a monomer is shown for clarity. Subunit qcrA is highlighted in *red*, qcrB in *magenta* and subunit qcrC in *yellow*. The heme groups are shown in sphere representation and SCR0911 in stick (*green*). The iron-sulfur cluster in subunit qcrA is shown as *red sphere*. (inset) The interaction profile of the SCR0911 with the *Mtb* cyt-*bcc* complex residues. (B) Zoomed in view of 1st major docked complex configuration of *Mtb* cyt-*bcc* with SCR0911 showing the proximity of the compound to the Q_o-site. The menaquinones are shown as line representation with the functional ones near Q_o-and Q_i-site in *red* and the others three in *green*. SCR0911 falls in the position of one of the menaquinone positions. The low and high spin hemes are marked. (C) Cartoon representation of the 2nd minor docked complex configuration of *Mtb* cyt-*bcc* with SCR0911. (inset) The interaction profile of the SCR0911 with the *Mtb* cyt-*bcc* complex residues. (D) Zoomed in view of 2nd minor docked complex configuration of *Mtb* cyt-*bcc* with SCR0911 showing the compound binding on the Q_i-site. The menaquinones are shown as line representation with the functional ones near Q_o-and Q_i-site in *red* and the others three in *green*. SCR0911 binds in the similar position as that of the

menaquinone in the Q_i-site. (E) Structural overlap of qcrB subunits of *Mtb* (*magenta*) and bovine (*grey*) cyt-*bcc* complex. The SCR0911 in the 2nd minor complex configuration of *Mtb* cyt-*bcc* is shown in *green* and the bound SCR0911 in the bovine cyt-*bcc* structure is shown as *grey stick* representation. Although the quinolone moiety binds at similar position, the trifluoromethoxyphenyl pyridine moiety orient in different direction showing a diffential binding.

Figure 3. Modified synthesis scheme for SCR0911.

Figure 4. Growth inhibition of BDQ (*black*) and SCR0911 (*blue*) in *M. smegmatis* (A), *M. bovis*_BCG (B), and_*M. smegmatis* Δ*bcc* mutant (C). The MIC_{50} values for BDQ in *M. smegmatis*, *M. bovis*_BCG, and *M. smegmatis* Δ*bcc* mutant are 17 nM, 188 nM and 16 nM, respectively, while the MIC_{50} values for SCR0911 in *M. smegmatis* and *M. bovis* BCG are 272 μM and 107 μM. A growth curve of the *M. smegmatis* Δ*bcc* mutant in the presence of increasing amounts of Telacebec (Q203) is shown in *red*. (D) Intracellular ATP synthesis assay of BDQ (*black*), Telacebec (Q203) (*red*) and SCR0911 (*blue*) in *M. bovis*_BCG indicates an IC_{50} of 29 nM, 0.5 nM and 50 μM, respectively. Error bars represents the standard deviations. The experiment has been carried out on two biological replicates.

Figure 5. Inhibition of ATP synthesis by SCR0911 in IMVs from *M. smegmatis* demonstrates an IC_{50} of 7.6 μM (A) and 6.9 μM in *M. bovis* BCG (B). Inhibition of ATP synthesis by SCR0911 and Telacebec (Q203) in PMVs from *M. smegmatis* using NADH as a donor (C) portrays an IC_{50} of 3.8 μM and 1.1 nM, respectively, while the PMVs from *M. smegmatis* using succinate as a donor (D) portrays an IC_{50} of 3.4 μM and 2.0 nM,

respectively. Error bars represents the standard deviations. The experiment has been carried out on two biological replicates.

Figure 6. Oxygen consumption assay with methylene blue as an indicator with *M. smegmatis* in the presence of SCR0911. The 7H9 sample contains only the 7H9 media and served as a blank. The drug free (DF) sample, containing the untreated *M. smegmatis* cells, served as the negative control, while THZ was used as positive control. (A) Visual representation of one representative replicate of the tubes at the various conditions was shown. (B) A bar chart of percent decolorization was plotted for *M. smegmatis*, indicating the effectiveness of SCR0911 in inhibiting oxygen respiration. Error bars represents the standard deviation. Error bars represents the standard deviation. The experiment has been carried out on two biological replicates.

Figure 7. Substrate-driven proton pumping in WT *M. smegmatis* PMVs with NADH as the substrate, demonstrating no major uncoupling effect with 15 uM of SCR0911. The experiment has been carried out on three biological replicates.

FOR TABLE OF CONTENTS ONLY

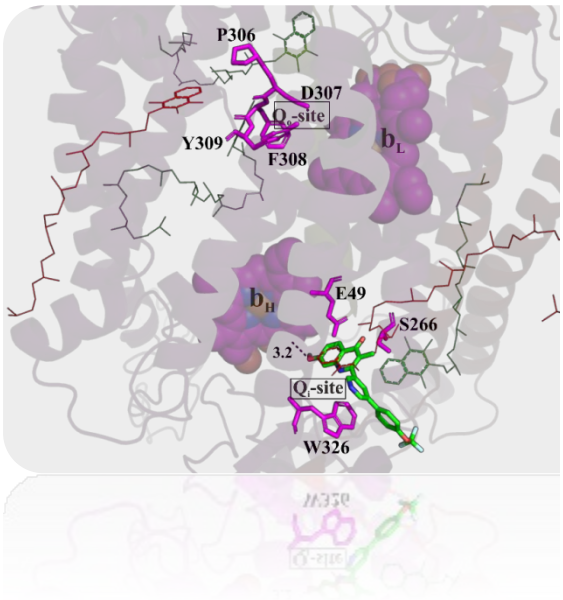

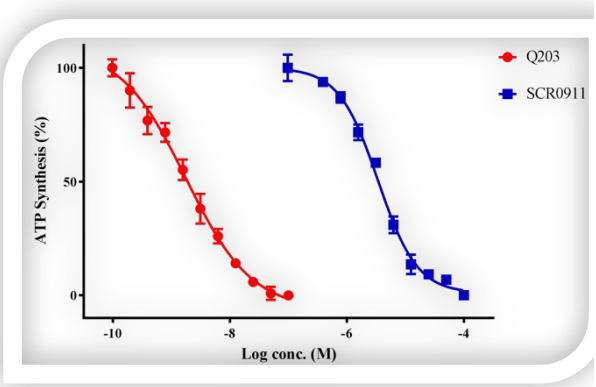

SCR0911

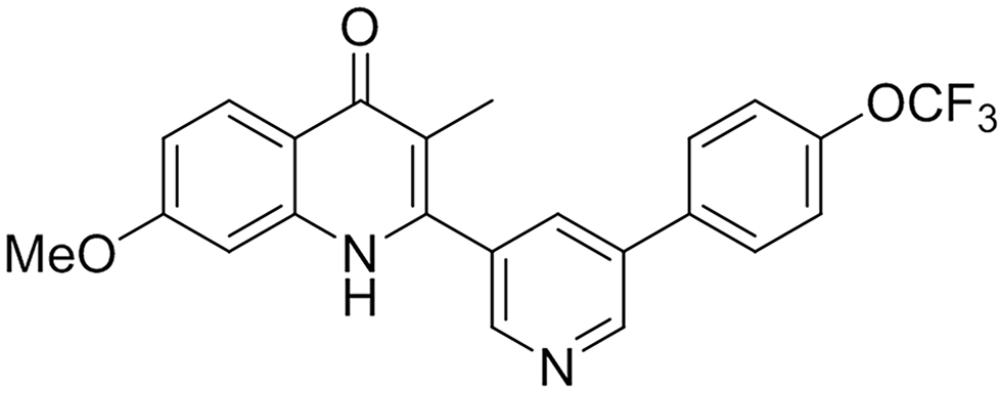

Figure 1A

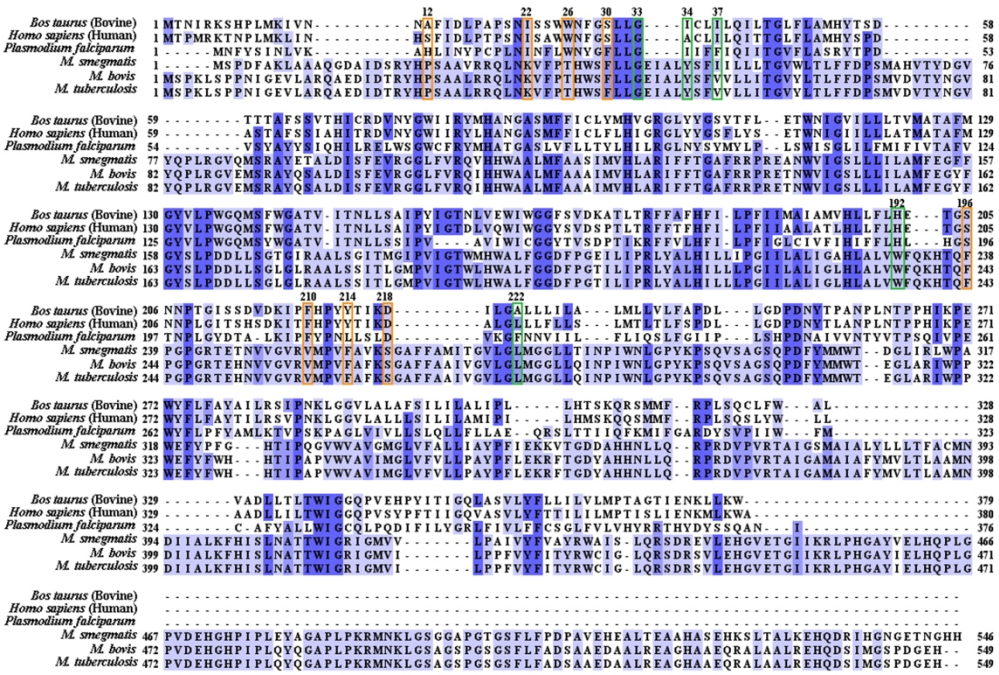
Bos taurus (Bovine)
Homo sapiens (Human)
Plasmodium falciparum
M. smegmatis
M. bovis
M. tuberculosis

Figure 1B

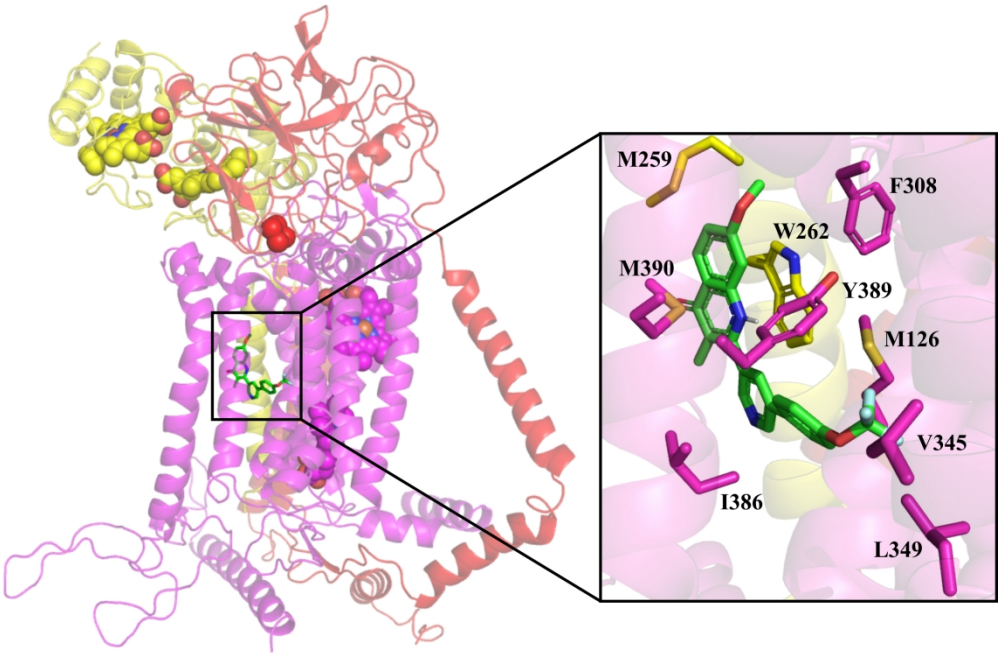

Figure 2A

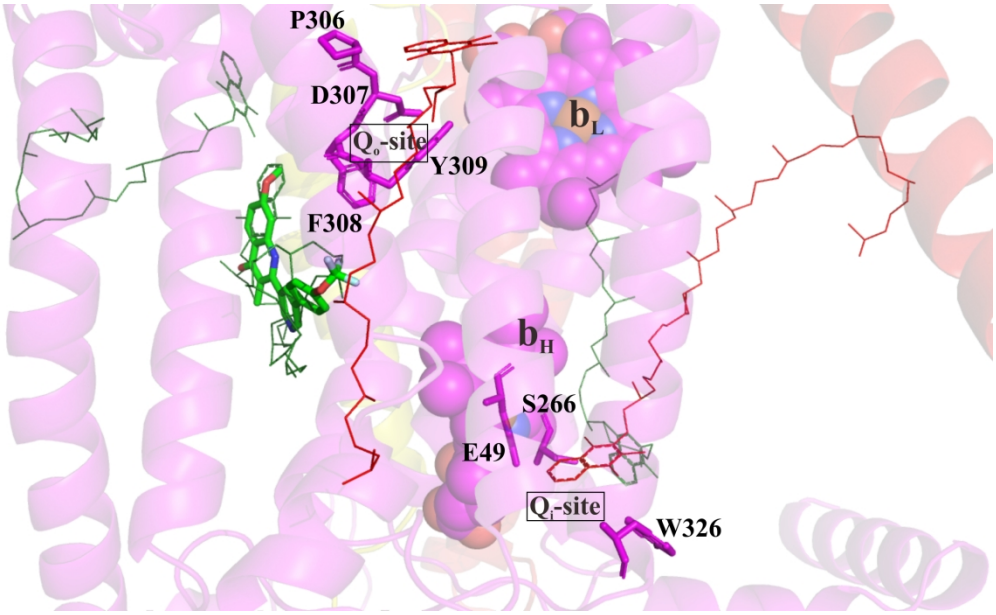

Figure 2B

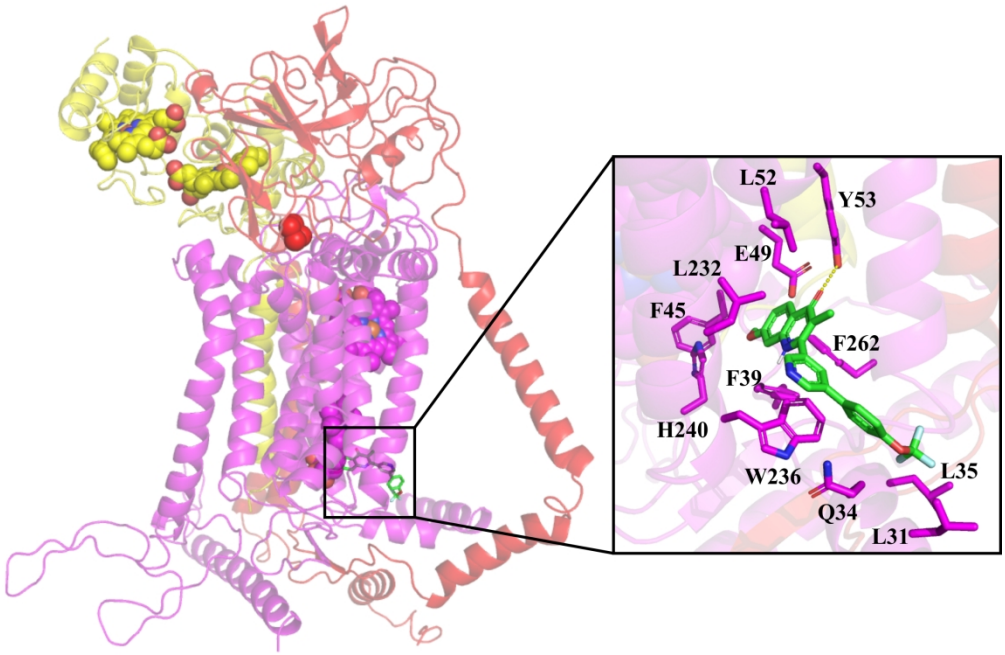

Figure 2C

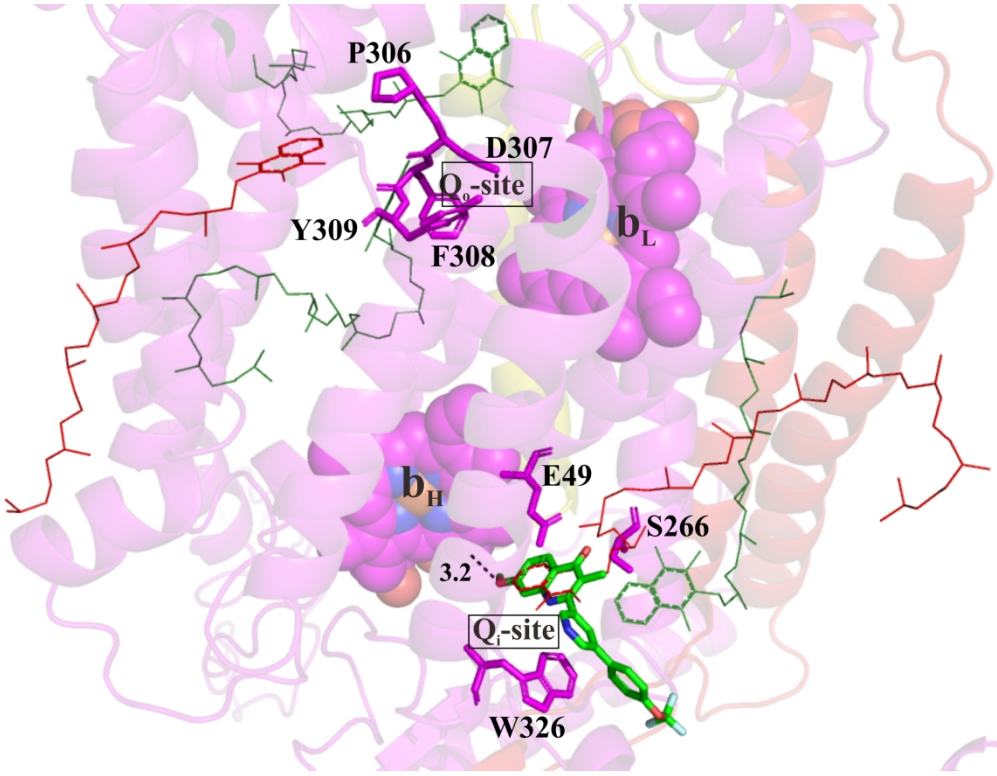

Figure 2D

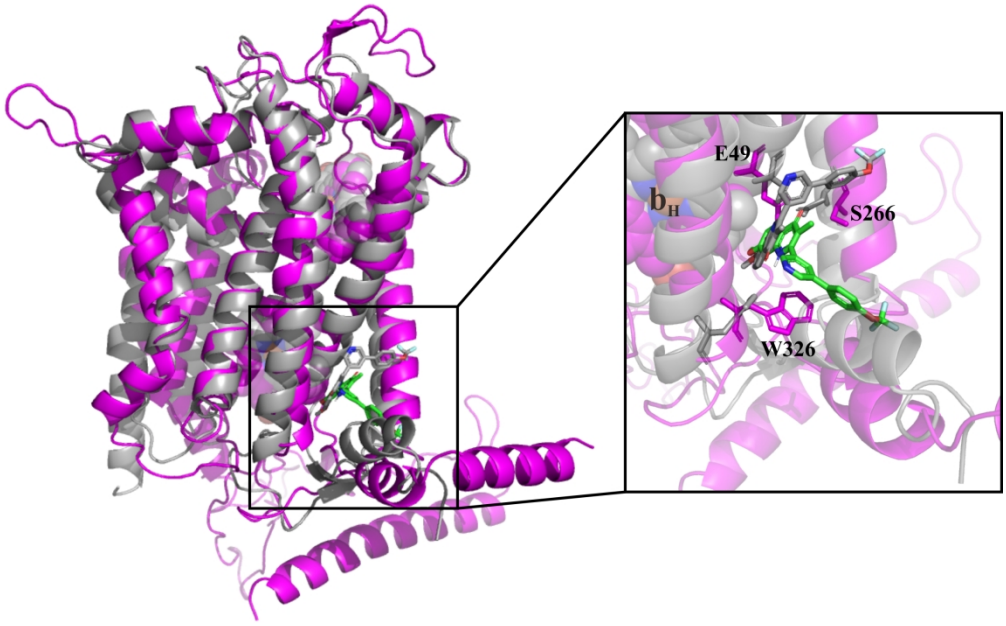

Figure 2E

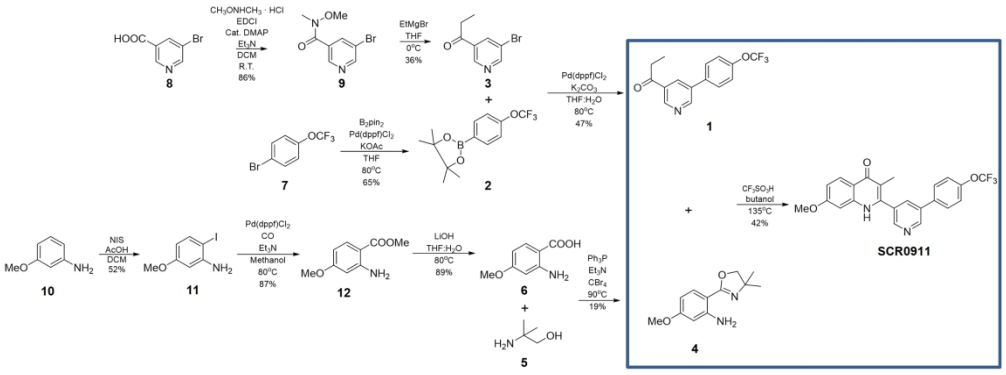

Figure 3

217x81mm (300 x 300 DPI)

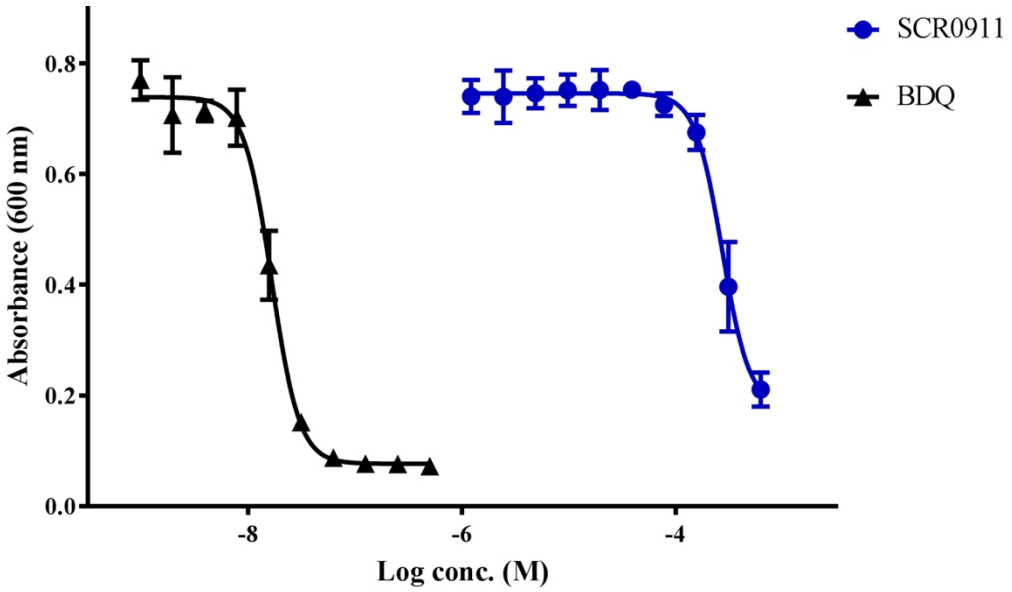

Figure 4A

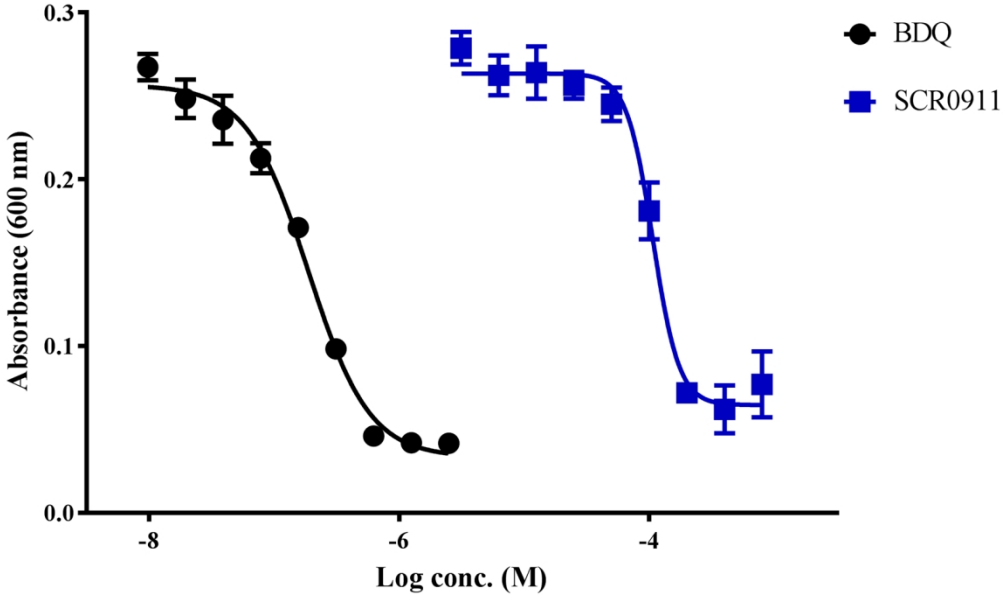

Figure 4B

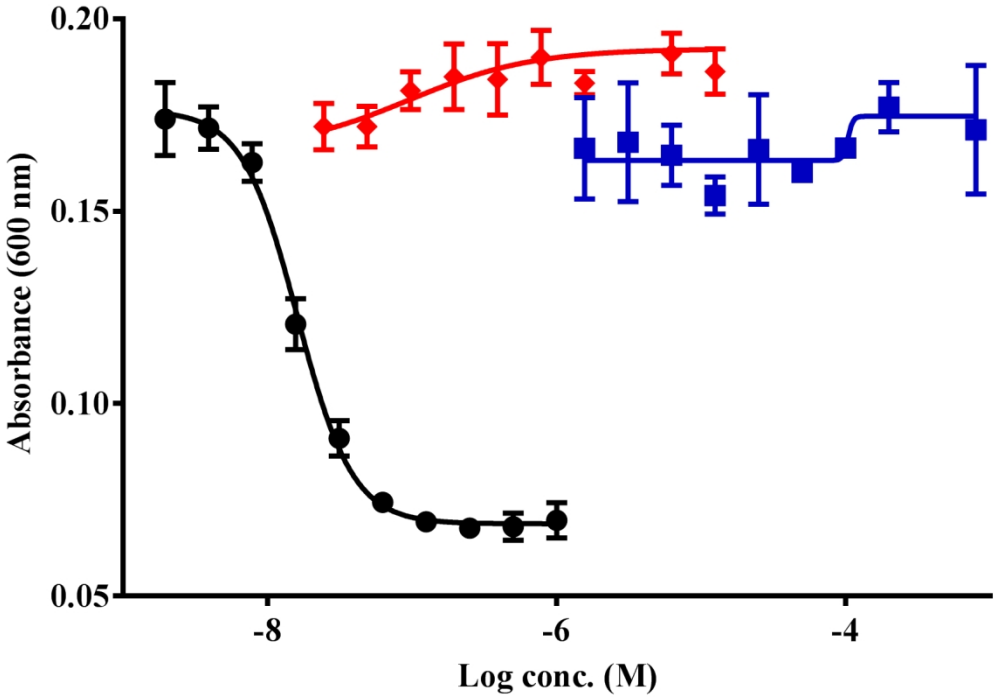

Figure 4C

145x101mm (300 x 300 DPI)

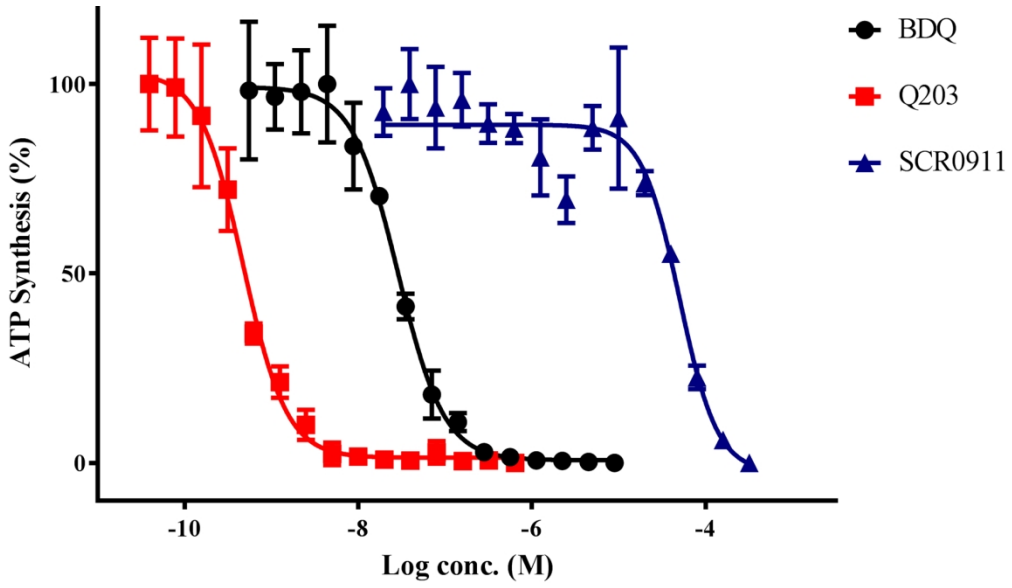

Figure 4D

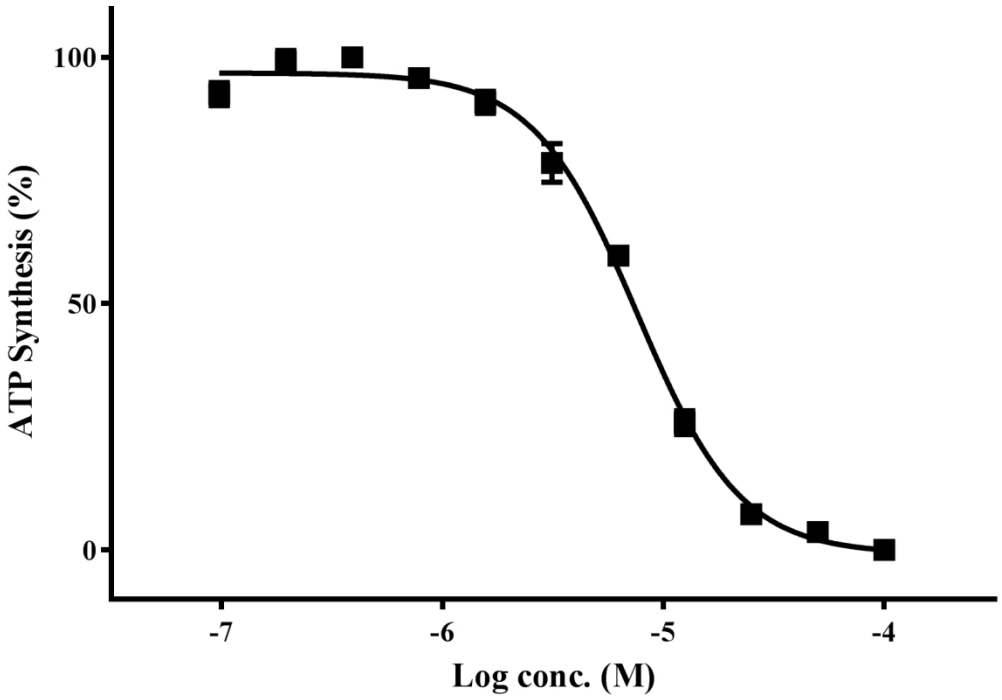

Figure 5A

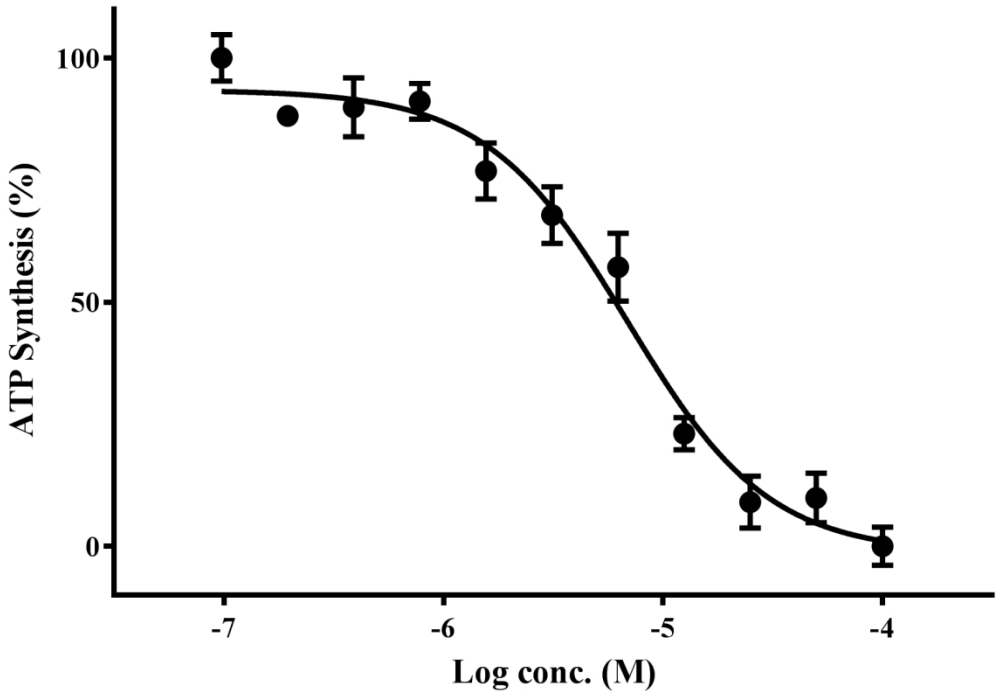

Figure 5B

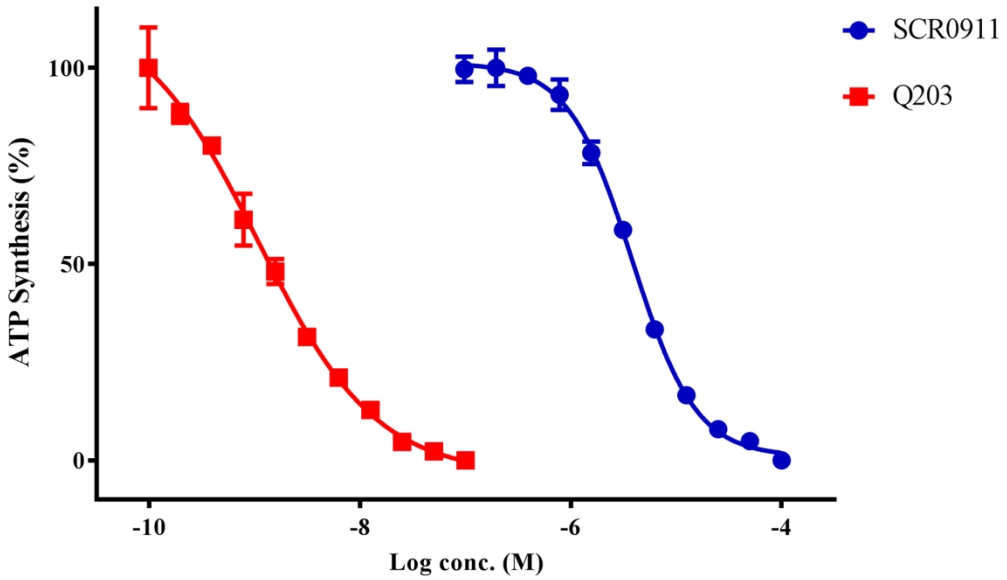

Figure 5C

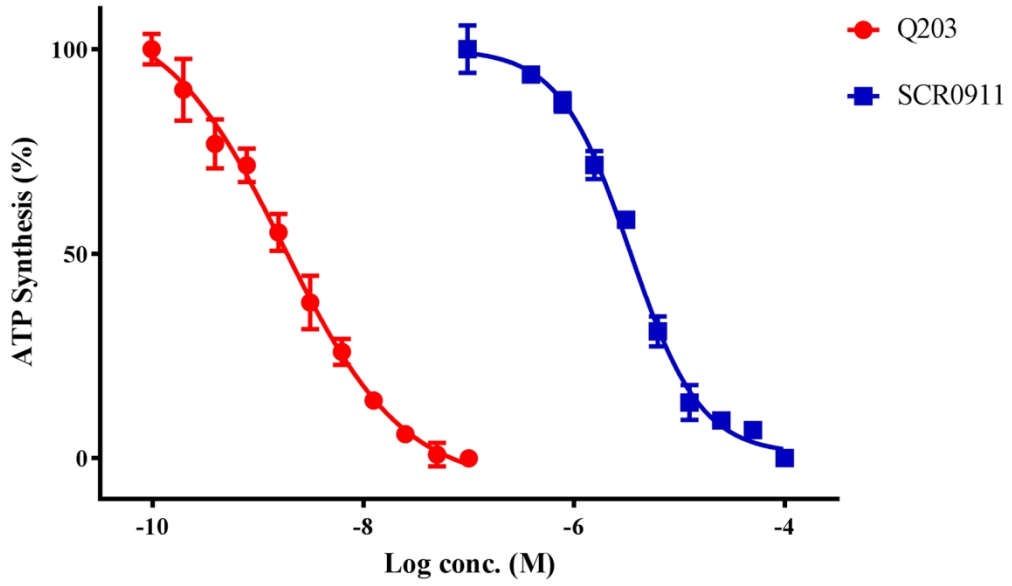

Figure 5D

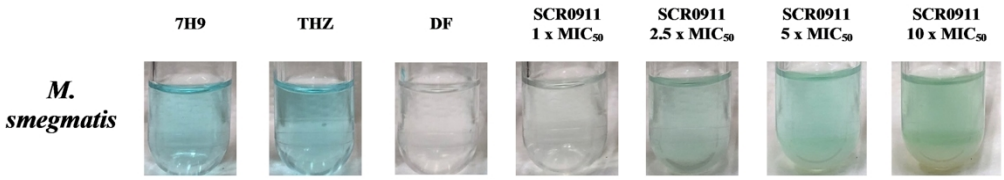
7H9
THZ
DF
SCR0911 1 x MIC50
SCR0911 2.5 x MIC50
SCR0911 5 x MIC50
SCR0911 10 x MIC50
M. smegmatis

Figure 6A

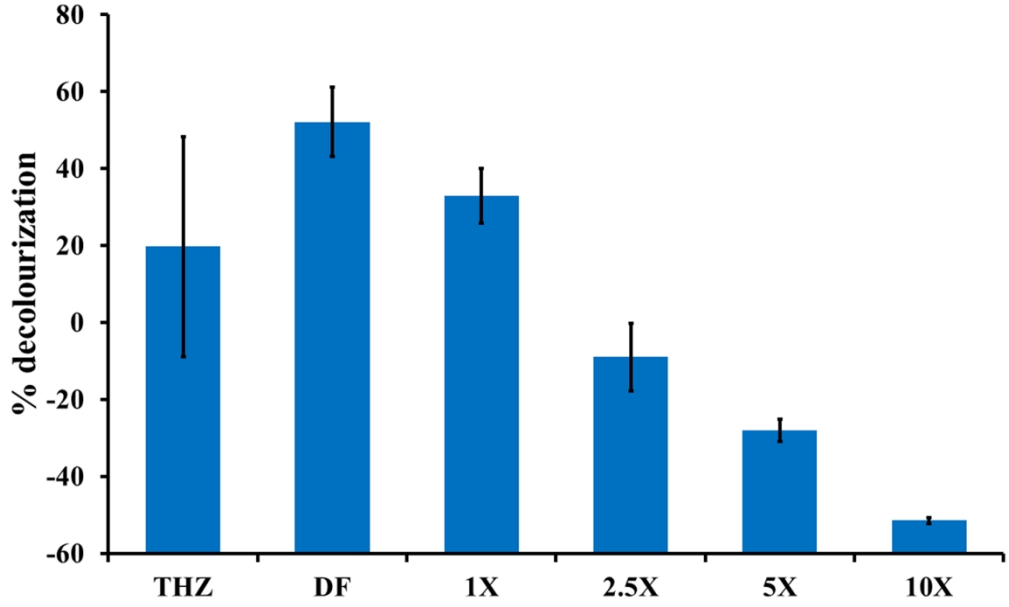

Figure 6B

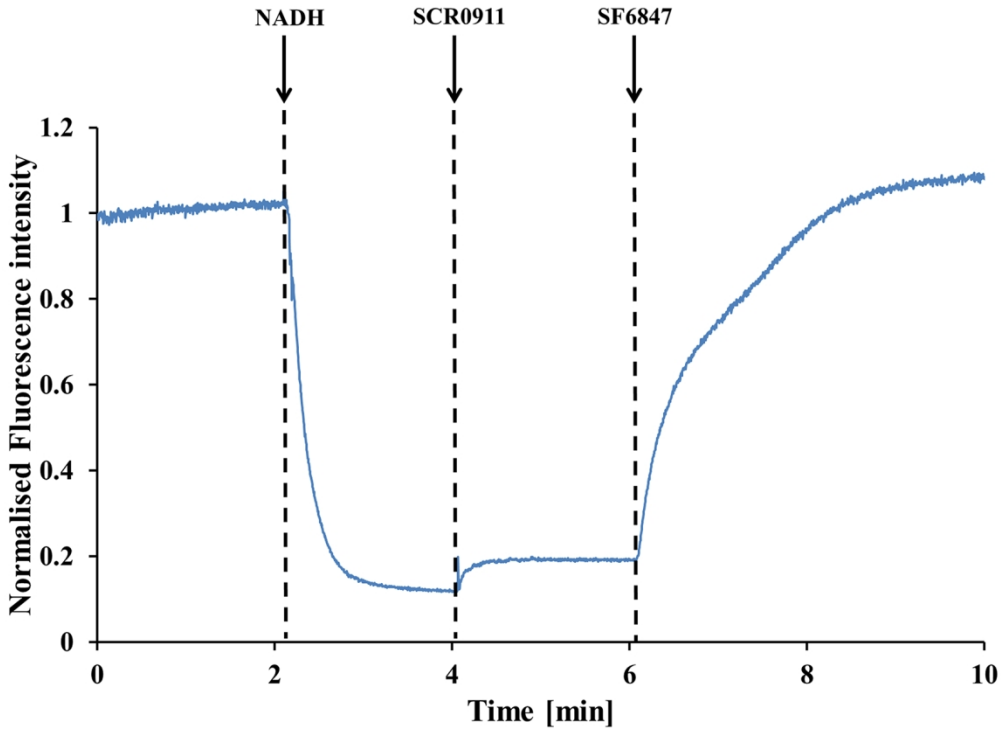
NADH
SCR0911
SF6847
Normalised Fluorescence intensity
1.2
1
0.8
0.6
0.4
0.2
0
0
2
4
6
8
10
Time [min]

Figure 7